

Synthesis, Structure, and H₂O₂-Dependent Catalytic Functions of Disulfide-Bridged Dicopper(I) and Related Thioether–Copper(I) and Thioether–Copper(II) Complexes

Takehiro Ohta,[†] Takashi Tachiyama,[†] Kazunari Yoshizawa,^{*,†} Tokio Yamabe,[‡] Takeshi Uchida,[§] and Teizo Kitagawa^{*,§}

Department of Molecular Engineering, Kyoto University, Sakyo-ku, Kyoto 606-8501, Japan, Institute for Fundamental Chemistry, 34-4 Takano-Nishihiraki-cho, Sakyo-ku, Kyoto 606-8103, Japan, and Institute for Molecular Science, Okazaki National Research Institutes, Myodaiji-cho, Okazaki 444-8585, Japan

Received January 5, 2000

A disulfide-bridged dicopper(I) complex, [Cu₂(Py₂SSPy₂)](ClO₄)₂ (**1**) (Py₂SSPy₂ = bis{2-[*N,N*-bis(2-pyridylethyl)-amino]-1,1-dimethylethyl}disulfide), a thioether–copper(I) complex, [Cu(ⁱPrSPy₂)](ClO₄) (**2**) (ⁱPrSPy₂ = *N*-(2-isopropylthio-2-methylpropyl)-*N,N*-bis-2-(2-pyridyl)ethylamine), and a thioether–copper(II) complex, [Cu(PheSPy₂)(H₂O)](ClO₄)₂ (**3**) (PheSPy₂ = *N*-(2-methyl-2-phenethylthio)propyl-*N,N*-bis-2-(2-pyridyl)ethylamine), were newly synthesized by the reactions of Cu(ClO₄)₂·6H₂O with a thiol ligand of Py₂SH (*N,N*-bis[2-(2-pyridyl)ethyl]-1,1-dimethyl-2-mercaptoethylamine) and thioether ligands of ⁱPrSPy₂ and PheSPy₂, respectively. For complexes **1** and **2**, X-ray analyses were performed. Complex **1** crystallizes in the triclinic space group *P*₁, and complex **2** crystallizes in the orthorhombic space group *Pbca* with the following unit cell parameters: for **1**, *a* = 15.165 (3) Å, *b* = 22.185 (4) Å, *c* = 14.989 (3) Å, α = 105.76 (1)°, β = 90.82 (2)°, γ = 75.23 (1)°, and *Z* = 2; for **2**, *a* = 17.78 (2) Å, *b* = 17.70 (1) Å, *c* = 15.75 (1) Å, and *Z* = 8. Complex **1** is the first structurally characterized example obtained by the redox reaction Cu(II) + RSH → Cu(I) + RSSR and has two independent structures (**1a**, **1b**) which mainly differ in S–S bond distances, Cu(I)···Cu(I) separations, and C–S–S–C dihedral angles of the disulfide units. The S–S bond distances of 2.088(7) Å in **1a** and 2.070(7) Å in **1b** are indicative of significant activation of the S–S bonds by the dicopper centers. Fragment molecular orbital (FMO) analyses and molecular orbital overlap population (MOOP) analyses based on the extended Hückel method clarify the preferable formation of the disulfide S–S bond in **1** rather than the formation of a thiolate–copper(II) complex within the Py₂S[−] ligand framework. Catalytic functions of complexes **1–3** were investigated with peroxides (H₂O₂ and ^tBuOOH) as oxidants. Complex **1** catalyzed the selective oxidation of cyclohexane to cyclohexanol and mediated the cyclohexene epoxidation in the presence of H₂O₂. A transient dark green intermediate observed in the reaction of **1** with H₂O₂ is characterized by UV–vis, EPR, and resonance Raman spectroscopies, identifying it as a Cu(II)–OOH species, **1**(OOH). The resonance Raman features of the ν(O–O) bands at 822 and 836 cm^{−1}, which are red-shifted to 781 and 791 cm^{−1}, respectively, upon introduction of H₂¹⁸O₂, are indicative of formation of two kinds of Cu–OOH species rather than the Fermi doublet and the significant weakening of the O–O bonds. These mechanistic studies demonstrate that by virtue of the electron-donating ability of the disulfide unit the Cu–OOH species can be actually activated for one-electron oxidation, which has been reported so far unfavorable for other vibrationally characterized Cu–OOH species.

Introduction

Dioxygen–copper interactions are key steps for the metabolic functions of copper monooxygenases.^{1,2} Much of the attention in bioinorganic functional modeling of copper proteins involved in O₂ use has focused on the dinuclear copper enzymes of hemocyanin and tyrosinase, which bind and activate dioxygen on the dinuclear framework, and there has been considerable progress in the understanding of dicopper–dioxygen species.^{3–5}

However, dopamine β-monooxygenase (DβM),^{2b,6–8} which catalyzes the hydroxylation of dopamine at the benzylic position

[†] Kyoto University.

[‡] Institute for Fundamental Chemistry.

[§] Okazaki National Research Institute.

- (1) (a) Linder, M. C.; Goode, C. A. *Biochemistry of Copper*; Plenum: New York, 1991. (b) Kaim, W.; Schwederski, B. *Bioinorganic Chemistry: Inorganic Elements in the Chemistry of Life*; Wiley: New York, 1994. (c) *Bioinorganic Chemistry of Copper*; Karlin, K. D., Tyeklar, Z., Eds.; Chapman & Hall: New York, 1993.
- (2) (a) Holm, R. H.; Kennepohl, P.; Solomon, E. I. *Chem. Rev.* **1996**, *96*, 2239. (b) Klinman, J. P. *Chem. Rev.* **1996**, *96*, 2541. (c) Solomon, E. I.; Sundaram, U. K.; Machonkin, T. E. *Chem. Rev.* **1996**, *96*, 2563. (d) Stubbe, J.; van der Donk, W. A. *Chem. Rev.* **1998**, *98*, 705.

- (3) For reviews see: (a) Karlin, K. D.; Gultneh, Y. *Prog. Inorg. Chem.* **1987**, *35*, 219. (b) Tyeklar, Z.; Karlin, K. D. *Acc. Chem. Res.* **1989**, *22*, 241. (c) Karlin, K. D.; Tyeklar, Z. *Adv. Inorg. Biochem.* **1993**, *9*, 123. (d) Murthy, N. N.; Karlin, K. D. In *Mechanistic Bioinorganic Chemistry*; Thorp, H. H., Pecoraro, V. L., Eds.; American Chemical Society: Washington, DC, 1995. (e) Kitajima, N.; Moro-oka, Y. *Chem. Rev.* **1994**, *94*, 737. (f) Karlin, K. D.; Kaderki, S.; Zuberbühler, A. D. *Acc. Chem. Res.* **1997**, *30*, 139. (g) Tolman, W. B. *Acc. Chem. Res.* **1997**, *30*, 227.
- (4) (a) Cole, A. P.; Root, D. E.; Mukherjee, P.; Solomon, E. I.; Stack, T. D. P. *Science* **1996**, *273*, 1848. (b) DuBois, J. L.; Mukherjee, P.; Collier, A. M.; Mayer, J. M.; Solomon, E. I.; Hedmon, B.; Stack, T. D. P.; Hodgson, K. O. *J. Am. Chem. Soc.* **1997**, *119*, 8578. (c) Mahadevan, V.; Hou, Z.; Cole, A. P.; Root, D. E.; Lal, T. K.; Solomon, E. I.; Stack, T. D. P. *J. Am. Chem. Soc.* **1997**, *119*, 11996.
- (5) (a) Itoh, S.; Kondo, T.; Komatsu, M.; Ohshiro, Y.; Li, C.; Kanehisa, N.; Kai, Y.; Fukuzumi, S. *J. Am. Chem. Soc.* **1995**, *117*, 4714. (b) Itoh, S.; Nakao, H.; Berreau, L. M.; Kondo, T.; Komatsu, M.; Fukuzumi, S. *J. Am. Chem. Soc.* **1998**, *120*, 2890.
- (6) (a) Brenner, M. C.; Klinman, J. P. *Biochemistry* **1989**, *28*, 249. (b) Tian, G.; Berry, J. A.; Klinman, J. P. *Biochemistry* **1994**, *33*, 226.

to norepinephrine, and peptidylglycine α -hydroxylating monooxygenase (PHM),^{9–11} which mediates the stereospecific hydroxylation of the glycine α -carbon of peptidylglycine substrates, are a new class of copper enzymes, in that the dioxygen binding and the substrate hydroxylation are carried out on one copper center, called Cu_B, of the dicopper active site, and a new paradigm for the activation of dioxygen and C–H bonds is required. A recent X-ray analysis⁹ showed that methionine (MetS) is coordinating to the Cu_B site of PHM, and preparation and characterization of half-apo-reduced D β M⁷ demonstrated the coordination of an S-donor, presumably MetS, to the Cu_B center. Therefore, to elucidate the mechanisms of the enzymatic activation of dioxygen and C–H bonds, which may be strongly dependent on the unclear roles of an S-donor, it is of importance to perform mechanistic studies for the dioxygen–copper chemistry carried out by a copper model involving an S-donor ligand. The reactivity of a copper monooxygenase model involving a thioether ligand has been investigated by Casella and co-workers.¹² They synthesized dicopper(I) complexes with three N₄-donor ligands and an N₂S₂-donor ligand and investigated the reaction rates of the ligand hydroxylation that occurred by exposing the dicopper(I) complexes to dioxygen. They have found that the S-donor coordination to the Cu(I) centers decreases the reaction rate of the ligand hydroxylation due to the stabilization of the copper(I) state. Réglie and co-workers¹³ found that an oxygen atom transfer to an S atom of a thioether moiety of a ligand occurs in a thioether–copper(II) complex when the complex is treated with H₂O₂. Despite their pioneering work for the ligand oxidations, the study for the activation of C–H bonds of hydrocarbons catalyzed by a copper–sulfur complex is still lacking, particularly concerning the oxidation mechanism of D β M and PHM.

In our effort to obtain copper–sulfur compounds as possible models for the copper monooxygenases, we have previously reported¹⁴ the synthesis of the disulfide-bridged dicopper(I) complex [Cu₂(Py₂SSPy₂)(ClO₄)₂] (**1**) (Py₂SSPy₂ = bis{2-[N,N-bis(2-pyridylethyl)amino]-1,1-dimethylethyl}disulfide)), which demonstrated the H₂O₂-dependent oxidation functions. Furthermore, we observed a transient dark green species in the reaction of **1** with H₂O₂ in CH₃CN. We present here characterizations of **1** by single-crystal X-ray analyses, UV–vis and NMR spectroscopies, and extended Hückel calculations and report resonance Raman studies for the transient dark green intermediate in the **1**/H₂O₂ system. A related thioether–copper(I) complex, [Cu(PrSPy₂)(ClO₄)₂] (**2**) (PrSPy₂ = N-(2-isopropylthio-2-methyl)propyl-N,N-bis-2-(2-pyridyl)ethylamine), and a thioether–copper(II) complex, [Cu(PheSPy₂)(H₂O)](ClO₄)₂ (**3**) (PheSPy₂ = N-(2-methyl-2-phenethylthio)propyl-N,N-bis-2-(2-pyridyl)ethylamine), were newly synthesized by the reaction of Cu(ClO₄)₂·6H₂O with corresponding ligands and subjected to

structural and spectroscopic characterizations. Catalytic functions of **2** and **3** with peroxides were also investigated in comparison with **1**.

Experimental Section

Materials. Most reagents were of the best commercial grade and were used without further purification. Hydrogen peroxide (H₂O₂) (30% in H₂O) and *tert*-butyl hydroperoxide (tBuOOH) (70% in H₂O) were titrated by iodometry. H₂¹⁸O₂ was synthesized following the literature method.¹⁵ The ratio H₂¹⁸O₂:H₂¹⁶O₂ was determined to be 7:3 by the product analyses for the styrene epoxidation carried out by myoglobin¹⁶ with prepared H₂¹⁸O₂ as an oxidant. The concentration of aqueous H₂¹⁸O₂ was determined to be 500 mM by an iodometry titration. Elemental analyses were carried out at the Microanalysis Center, Kyoto University.

Safety Note. *Caution! Perchlorate salts of metal complexes with organic ligands are potentially explosive. Only small amounts of material should be prepared, which should be handled with great care.*

N,N-Bis[2-(2-pyridyl)ethyl]-1,1-dimethyl-2-mercaptoethylamine (Py₂SH). Bis[2-(2-pyridyl)ethyl]amine¹⁷ (9.00 g, 39.6 mmol) and isobutylene sulfide¹⁸ (3.50 g, 39.7 mmol) were stirred at 70 °C for 24 h. The reaction mixture was extracted with AcOEt. After removal of the solvent the residual oil was purified by flash column chromatography (SiO₂, AcOEt–MeOH, 7:1, v/v). A pale yellow viscous oil of Py₂SH was obtained (6.10 g, 48.8% yield). Anal. Calcd for C₁₈H₂₅N₃S: C, 68.53; H, 7.99; N, 13.32; S, 10.16. Found: C, 68.37; H, 7.98; N, 13.06; S, 10.15. ¹H NMR data (δ /ppm vs TMS) in CDCl₃: 8.52 (d, *J* = 4.9 Hz, 2H), 7.58 (t, *J* = 6.8 Hz, 2H), 7.16 (d, *J* = 7.8 Hz, 2H), 7.10 (d, *J* = 6.3 Hz, 2H), 3.13–2.97 (m, 8H), 2.63 (s, 2H), 1.23 (s, 6H).

N-(2-Isopropylthio-2-methyl)propyl-N,N-bis-2-(2-pyridyl)ethylamine (PrSPy₂). To a stirred solution of Py₂SH (2.00 g, 6.34 mmol) in THF sodium was slowly added sodium (0.146 g, 6.35 mmol). The solution was refluxed until the sodium block was dissolved, and subsequently the reaction mixture turned to a pale yellow suspension. To the resulting solution was added dropwise isopropyl iodide (1.08 g, 6.35 mmol), giving an orange solution of the reaction mixture. After the reaction mixture was cooled, Et₂O was added and a precipitated white solid was filtered. The filtrate was extracted with Et₂O (20 mL \times 3), and the combined extracts were dried over anhydrous Na₂SO₄. The solvent was evaporated and purified by silica gel column chromatography (AcOEt–MeOH, 7:1, v/v), giving PrSPy₂ as an orange viscous oil (1.66 g, 72.0% yield). Anal. Calcd for C₂₁H₃₁N₃S: C, 70.54; H, 8.74; N, 11.75; S, 8.97. Found: C, 70.66; H, 8.74; N, 11.55; S, 9.23. ¹H NMR data (δ /ppm vs TMS) in CDCl₃: 8.52 (d, *J* = 3.9 Hz, 2H), 7.58 (t, *J* = 7.6 Hz, 2H), 7.17 (d, *J* = 7.8 Hz, 2H), 7.11 (d, *J* = 6.4 Hz, 2H), 3.09–2.93 (m, 8H), 2.67 (s, 2H), 1.26 (d, *J* = 6.8 Hz, 6H), 1.20 (s, 6H).

N-(2-Methyl-2-phenethylthio)propyl-N,N-bis-2-(2-pyridyl)ethylamine (PheSPy₂). To a stirred solution of Py₂SH (0.5 g, 1.58 mmol) in THF sodium was slowly added sodium (36.5 mg, 1.59 mmol). The solution was refluxed until the sodium block was dissolved, and subsequently the reaction mixture turned to a pale yellow suspension. To the resulting solution was added dropwise 2-bromoethylbenzene (0.29 g, 1.57 mmol), giving an orange solution of the reaction mixture. After the reaction mixture was cooled, Et₂O was added and a precipitated white solid was filtered. The filtrate was extracted with Et₂O (10 mL \times 3), and the combined extracts were dried over anhydrous Na₂SO₄. The solvent was evaporated and purified by silica gel column chromatography (AcOEt–MeOH, 7:1, v/v), giving PheSPy₂ as an orange viscous oil (0.494 g, 69.9% yield). Anal. Calcd for C₂₆H₃₃N₃S: C, 74.42; H, 7.93; N, 10.01. Found: C, 74.37; H, 8.02; N, 10.07. ¹H NMR data (δ /ppm vs TMS) in CDCl₃: 8.51 (d, *J* = 4.9 Hz, 2H), 7.56 (t, *J* = 7.7 Hz,

- (7) Reedy, B. J.; Blackburn, N. J. *J. Am. Chem. Soc.* **1994**, *116*, 1924.
 (8) Padgett, S. R.; Wimalasena, K.; Herman, H. H.; Sirimanne, S. R.; May, S. W. *Biochemistry* **1985**, *24*, 5826.
 (9) Prigge, S. T.; Kolhekar, A. S.; Eipper, B. A.; Mains R. E.; Amzel, L. M. *Science* **1997**, *278*, 1300.
 (10) Boswell, J. S.; Reedy, B. J.; Kulathila, R.; Merkler, D.; Blackburn, N. J. *Biochemistry* **1996**, *35*, 12241.
 (11) (a) Eipper, B. A.; Milgram, S. L.; Husten, E. J.; Yun, H.-Y.; Mains, R. E. *Protein Sci.* **1993**, *2*, 489. (b) Eipper, B. A.; Quon, A. S. W.; Mains, R. E.; Boswell, J. S.; Blackburn, N. J. *Biochemistry* **1995**, *34*, 2857.
 (12) Casella, L.; Gullotti, M.; Bartosek, M.; Pallanza, G.; Laurenti, E. *J. Chem. Soc., Chem. Commun.* **1991**, 1235.
 (13) Champloy, F.; Benali-Chérif, N.; Bruno, P.; Blain, I.; Pierrot, M.; Réglie, M.; Michalowicz, A. *Inorg. Chem.* **1998**, *37*, 3910.
 (14) Ohta, T.; Tachiyama, T.; Yoshizawa, K.; Yamabe, T. *Tetrahedron Lett.* **2000**, *41*, 2581.

- (15) Sawaki, Y.; Foote, C. S. *J. Am. Chem. Soc.* **1979**, *101*, 6292.
 (16) Ortiz de Montellano, P. R.; Catalano, C. E. *J. Biol. Chem.* **1985**, *260*, 9265.
 (17) Sanyal, I.; Mahroof-Tahir, M.; Nasir, M. S.; Gosh, P.; Cohen, B. I.; Gultneh, Y.; Cruse, R. W.; Farooq, A.; Karlin, K. D.; Liu, S.; Zubieta, J. *Inorg. Chem.* **1992**, *31*, 4322.
 (18) Sanders, M. *Chem. Rev.* **1966**, *66*, 297 and references therein.

2H), 7.28–7.06 (m, 9H), 3.08–2.94 (m, 8H), 2.80–2.74 (m, 4H), 2.65 (s, 2H), 1.19 (s, 6H).

[Cu₂(Py₂SSPy₂)](ClO₄)₂ (1). To a solution containing 1.0 g of Py₂SH (3.17 mmol) in 5 mL of methanol was added 5 mL of methanol solution in which 1.17 g of Cu(ClO₄)₂·6H₂O was dissolved, and the mixture was stirred for 30 min. The precipitated yellow solid was filtered and washed with Et₂O several times (1.18 g, 82%). UV–vis [CH₃CN, λ_{max}, nm (ε, M⁻¹ cm⁻¹): 263 (13 600), 300 (10 900). FAB mass (*m/z*): 855 ([Cu₂(Py₂SSPy₂)](ClO₄)⁺). Anal. Calcd for Cu₂C₃₆H₄₈N₆S₂Cl₂O₈: C, 45.28; H, 5.07; N, 8.80; Cl, 7.43. Found: C, 45.08; H, 5.07; N, 9.30; Cl, 7.34.

[Cu(ⁱPrSPy₂)](ClO₄) (2). To a solution containing 2.0 g of ⁱPrSPy₂ (5.59 mmol) in 5 mL of methanol was added, 5 mL of a methanol solution in which 2.07 g of Cu(ClO₄)₂·6H₂O was dissolved, and the mixture was stirred for 30 min. The mixture was then poured into a large amount of Et₂O. The resulting oily green material was separated and dissolved in 100 mL of CH₂Cl₂. Addition of Et₂O (100 mL) into the CH₂Cl₂ solution gave a green solid which was collected by filtration and washed with Et₂O several times. UV–vis [CH₃CN, λ_{max}, nm (ε, M⁻¹ cm⁻¹): 243 (9200), 308 (6800). FAB mass (*m/z*): 420 ([Cu(ⁱPrSPy₂)]⁺). Anal. Calcd for CuC₂₁H₃₁N₃SClO₄: C, 48.45; H, 6.00; N, 8.07; Cl, 6.81. Found: C, 48.45; H, 5.82; N, 8.07; Cl, 6.86.

[Cu(PheSPy₂)(H₂O)](ClO₄)₂ (3). To a solution containing 2.40 g of PheSPy₂ (5.72 mmol) in 5 mL of methanol was added 5 mL of methanol solution in which 2.17 g of Cu(ClO₄)₂·6H₂O was dissolved, and the mixture was stirred for 30 min. The mixture was then poured into a large amount of Et₂O. The resulting oily dark green material was separated and dissolved in 100 mL of CH₂Cl₂. Addition of Et₂O (100 mL) into the CH₂Cl₂ solution gave a blue-green solid, which was collected by filtration and washed with Et₂O several times. UV–vis [CH₃CN, λ_{max}, nm (ε, M⁻¹ cm⁻¹): 263 (11 300), 364 (3600), 685 (200). FAB mass (*m/z*): 482 ([Cu(PheSPy₂)]⁺). ESI mass (*m/z*): 482 ([Cu(PheSPy₂)]⁺). Anal. Calcd for CuC₂₆H₃₅N₃SClO₉: C, 44.61; H, 5.04; N, 6.00; Cl, 10.13. Found: C, 44.27; H, 4.93; N, 5.97; Cl, 9.94.

Catalytic Oxidation of Hydrocarbons. Oxidation of a hydrocarbon was conducted by employing 0.05 mmol of a complex and 1 mmol of a substrate with 0.5 mmol of H₂O₂ or ^tBuOOH in CH₃CN at room temperature under Ar or O₂ conditions. The reaction mixture was quenched with a saturated Na₂SO₄ solution, followed by extraction with 7 × 3 mL of Et₂O. Chlorobenzene (PhCl) was added at this point as an internal standard, and the reaction mixture was analyzed by GC (Shimadzu GC-18 A equipped with a flame ionization detector and a J & W Scientific DB-1701 chromatography column). Retention times and yields of products were confirmed by injections of authentic compounds.

Physical Methods. ¹H NMR spectra were recorded on either a JNM CSX-270 FT-NMR (270 MHz) or a JNM AL-300 FT-NMR (300 MHz) spectrometer, and chemical shifts were given relative to internal tetramethylsilane (TMS). Fast atom bombardment (FAB) mass spectra were measured using a Shimadzu/Kratos Concept IS mass spectrometer with xenon gas ionization in a matrix of *m*-nitrobenzyl alcohol (MNBA). The electrospray ionization (ESI) mass spectrum was obtained with a PE SCIEX API300 spectrometer. X-band electron paramagnetic resonance (EPR) spectral data were recorded on a JEOL JES-PE-2X ESR spectrometer in frozen CH₃CN solution at 77 K. UV–vis absorption spectra were measured in CH₃CN solutions with a Perkin-Elmer Lambda 19 spectrometer.

Resonance Raman samples of **1**(OOH) were prepared by adding an excess of H₂O₂ to a 0.3 mM [Cu₂(Py₂SSPy₂)](ClO₄)₂ solution in CH₃CN at –5 °C. Spectra were obtained by excitation with the 325 nm line of a He–Cd laser (Kinmon Electrics, model CD3041R). The scattering light at right angle was dispersed with a single polychromator (Ritsu Oyo Kogaku, DG-1000) and was detected with a Princeton Instruments liquid-N₂-cooled CCD detector (CCD-1340/400-EB). The Raman shifts were calibrated with acetone and acetonitrile, which were precalibrated with indene.

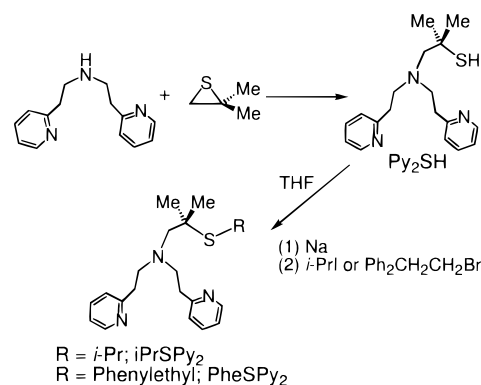
Crystallographic Data Collections. Crystals of complexes **1** and **2** were mounted onto glass fibers. Intensity data were collected on a Rigaku AFC-7R diffractometer with graphite-monochromated Mo Kα radiation (λ = 0.710 69 Å) at 296 K using the ω–2θ scan technique to a maximum 2θ value of 55°. The intensities of three representative

Table 1. Crystallographic Data for [Cu₂(Py₂SSPy₂)]₂(ClO₄)₂ (**1**)₂ and [Cu(ⁱPrSPy₂)](ClO₄) (**2**)^a

	(1) ₂	2
empirical formula	Cu ₄ C ₇₂ H ₉₆ N ₁₂ S ₄ Cl ₄ O ₁₆	Cu ₂ C ₂₁ H ₃₁ N ₃ SClO ₄
fw	1909.86	520.55
cryst syst	triclinic	orthorhombic
<i>a</i> , Å	15.165(3)	17.78(2)
<i>b</i> , Å	22.185(4)	17.70(1)
<i>c</i> , Å	14.989(3)	15.75(1)
α, deg	105.76(1)	
β, deg	90.82(2)	
γ, deg	75.23(1)	
<i>V</i> , Å ³	4684(1)	4958(12)
space group	<i>P</i> 1	<i>Pbca</i>
<i>Z</i>	2	8
<i>D</i> _{calcd} , g/cm ³	1.354	1.395
no. of reflns with <i>I</i> > 2σ(<i>I</i>)	7373	1815
refln/param ratio	7.31	6.48
<i>R</i> (<i>R</i> _w) ^{b,c} (%)	9.5 (12.5)	5.9 (6.1)

^a *T* = 293 K; Mo Kα radiation (λ = 0.7107 Å). ^b *R* = Σ(|*F*_o| – |*F*_c|)/Σ|*F*_o|. ^c *R*_w = {Σ[w(|*F*_o| – |*F*_c|)²]/Σ[w|*F*_o|²]}^{1/2}.

Scheme 1



reflections were measured every 150 reflections to ascertain crystal integrity, and no decay in intensity was observed. The data were collected for Lorenz and polarization effects. The structures were solved by a direct method (SHELX86)¹⁹ available on the TeXsan software package.^{20a} All non-hydrogen atoms were refined anisotropically, and hydrogen atoms were placed in calculated positions (*d*_{C–H} = 0.95). The atomic scattering factors were taken from the *International Tables for X-ray Crystallography*.^{20b} Pertinent crystallographic data and experimental conditions are summarized in Table 1.

Results and Discussion

Synthesis. The ligands were synthesized as shown in Scheme 1. To develop S-donor ligands, we employed the bis[2-(2-pyridyl)ethyl]amine unit as an N-donor framework, which has made significant contributions to the understanding of copper enzymes through their structural and functional modeling for dinuclear copper monooxygenases.^{5,17} Py₂SH was obtained by the ring-opening reaction of bis[2-(2-pyridyl)ethyl]amine and isobutylene sulfide under neat conditions at 70 °C. The deprotonation of Py₂SH by sodium yielded the moisture-sensitive sodium salt Py₂SNa, which was subsequently treated with isopropyl iodide and 2-bromoethylbenzene to give ⁱPrSPy₂ and PheSPy₂, respectively.

(19) SHELX86: Sherdrick, G. M. *Acta Crystallogr., Sect. A* **1990**, *46*, 467.

(20) (a) TeXsan: Single-Crystal Structure Analysis Software, Version 5.0, Molecular Structure Corp., The Woodlands, TX 77381, 1989. (b) *International Tables for X-ray Crystallography*; Kynoch Press: Birmingham, U.K., 1974; Vol. IV.

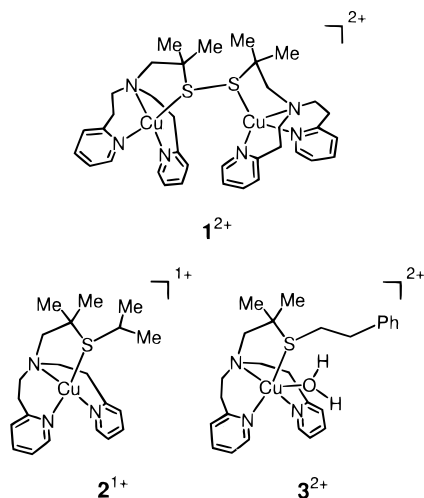
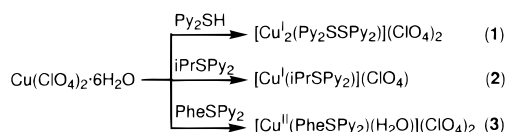


Figure 1. Schematic drawings of cations in complexes 1–3.

Scheme 2



The copper–sulfur complexes 1–3 were synthesized by the dropwise addition of the CH_3OH solution of $\text{Cu}(\text{ClO}_4)_2 \cdot 6\text{H}_2\text{O}$ to the corresponding ligands in CH_3OH solutions (Scheme 2). The schematic representations of the cationic parts in the complexes are shown in Figure 1. Interestingly, when Py_2SH was treated with the $\text{Cu}(\text{II})$ salt, we obtained the disulfide-bridged dicopper(I) complex $[\text{Cu}_2(\text{Py}_2\text{SSPy}_2)](\text{ClO}_4)_2$ (**1**). Complex **1** was stable for two weeks at room temperature, but it gradually decomposed to yield a green complex that is not characterized. During the dropwise addition of the CH_3OH solution of $\text{Cu}(\text{ClO}_4)_2 \cdot 6\text{H}_2\text{O}$ to that of Py_2SH , an intense green species at first appeared but was soon decolorized. Thus, at the initial step of the reaction between the $\text{Cu}(\text{II})$ salt and Py_2SH , a thiolate-coordinating complex of $[\text{Cu}^{\text{II}}(\text{Py}_2\text{S}^-)](\text{ClO}_4)$ would be formed, while the thiolate–copper(II) complex might be unstable, leading to the disulfide $\text{S}–\text{S}$ bond. When iPrSPy_2 was treated with the CH_3OH solution of $\text{Cu}(\text{ClO}_4)_2 \cdot 6\text{H}_2\text{O}$, despite employing the $\text{Cu}(\text{II})$ salt as a starting material, we obtained the air-stable monovalent complex $[\text{Cu}^{\text{I}}(\text{iPrSPy}_2)](\text{ClO}_4)$ (**2**).²¹ On the contrary, when the $\text{Cu}(\text{II})$ salt was treated with PheSPy_2 , the divalent complex **3** was formed. A preliminary X-ray analysis and an elemental analysis identified **3** as the divalent copper complex $[\text{Cu}^{\text{II}}(\text{PheSPy}_2)(\text{H}_2\text{O})](\text{ClO}_4)_2$. The FAB mass measurement showed a cation peak at m/z 482, corresponding to the $[\text{Cu}^{\text{I}}(\text{PheSPy}_2)]^+$ cation, and thereby under the FAB mass conditions the fifth (axial) ligand of water coordinating to the $\text{Cu}(\text{II})$ center in **3** may be easily removed, stabilizing the $\text{Cu}(\text{I})$ complex. Even by the more soft ionization method of ESI mass spectrometry, we also observed the $[\text{Cu}^{\text{I}}(\text{PheSPy}_2)]^+$ cation cluster peak at m/z 482, implying that the contribution of the reorganization barrier, included in the water ligand elimination,

(21) We cannot determine the reductant of the $\text{Cu}(\text{II})$ centers at the present stage, whereas there is a possibility that the thioether donor can be a reductant. The formation of an $\text{Fe}(\text{II})$ complex by the reaction of $\text{Fe}(\text{ClO}_4)_3$ with an N4-donor ligand was also reported in ref 36a, while a reductant for the initially formed $\text{Fe}(\text{II})$ complex was not specified. Thus, the reduction of metal centers during the formation of a complex with donor ligands seems to have occurred, while in many cases the determination of reductants in reaction mixtures should be difficult.

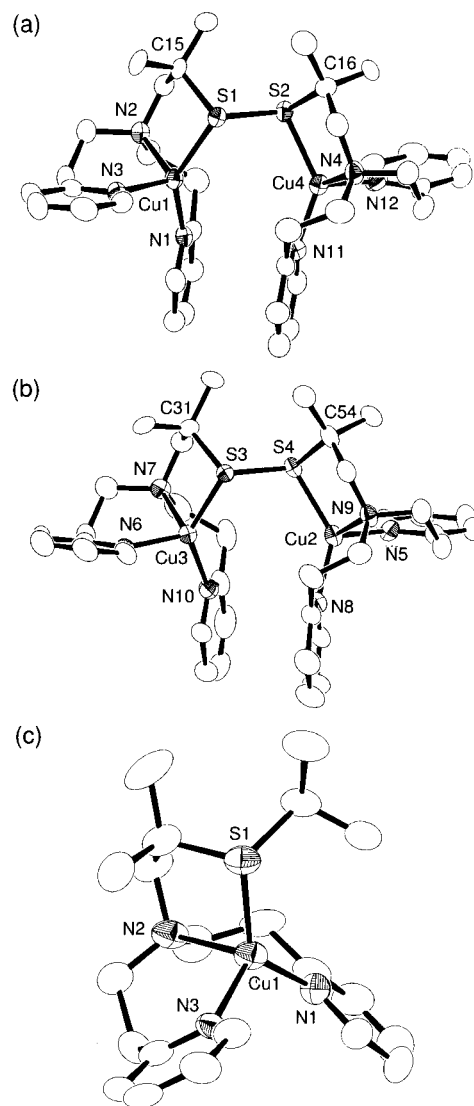


Figure 2. (a, b) ORTEP drawings (30% probability) of dications in **1a** and **1b**, respectively. (c) ORTEP drawing (30% probability) of a cation in **2**. Hydrogen atoms are omitted for clarity.

to the electron-transfer kinetics which describe the equilibrium between the $\text{Cu}(\text{II})$ and the $\text{Cu}(\text{I})$ states may be abnormally small in **3**.²²

Recently, Rorabacher and co-workers²² reported the influence of ligand coordination geometries upon $\text{Cu}(\text{I/II})$ redox potentials with 12 copper tripodal N,S-donor ligands. They determined $\text{Cu}(\text{II})$ complex stability constants ($K_{\text{Cu}^{\text{II}}\text{L}}$) and $\text{Cu}^{\text{II/I}}\text{L}$ potentials and calculated $\text{Cu}(\text{I})$ complex stability constants ($K_{\text{Cu}^{\text{I}}\text{L}}$) from $K_{\text{Cu}^{\text{II}}\text{L}}$ values and $\text{Cu}^{\text{II/I}}\text{L}$ potentials. From the $K_{\text{Cu}^{\text{II}}\text{L}}$ and $K_{\text{Cu}^{\text{I}}\text{L}}$ values determined with the utilization of BPMEEA and BPPEEA, congeners of our thioether ligands, they found that the $\text{Cu}(\text{I})$ complex is more stabilized than the $\text{Cu}(\text{II})$ complex with $\log K_{\text{Cu}^{\text{I}}\text{L}} \approx 14$ and $\log K_{\text{Cu}^{\text{II}}\text{L}} \approx 9$ for both the ligands. These results are consistent with our finding of the formation of the thioether–copper(I) complex from the reaction of the $\text{Cu}(\text{II})$ salt with iPrSPy_2 .

Crystal Structures. Single crystals of **1** and **2** were obtained by Et_2O diffusion into the acetone solutions containing the complexes. Complex **1** was crystallized in the space group $P\bar{1}$.

(22) Ambundo, E. A.; Deydier, M.-V.; Grall, A. J.; Aguera-Vega, N.; Dressel, L. T.; Cooper, T. H.; Heeg, M. J.; Ochrymowycz, L. A.; Rorabacher, D. B. *Inorg. Chem.* **1999**, *38*, 4233.

Table 2. Selected Bond Lengths, Bond Angles, and Dihedral Angles for [Cu₂(Py₂SSPy₂)](ClO₄)₂ (**1a**, **1b**) and [Cu(PrSPY₂)](ClO₄) (**2**)

Bond Lengths (Å)						
	1a		1b		2	
Cu–S	(Cu1–S1)	2.228(6)	(Cu2–S4)	2.242(6)	(Cu1–S1)	2.249(3)
	(Cu4–S2)	2.246(6)	(Cu3–S3)	2.246(6)		
Cu–N _{amine}	(Cu1–N2)	2.18(2)	(Cu2–N9)	2.17(2)	(Cu1–N2)	2.173(9)
	(Cu4–N4)	2.19(2)	(Cu3–N7)	2.17(2)		
Cu–N _{py}	(Cu1–N1)	2.00(2)	(Cu2–N5)	2.02(2)	(Cu1–N1)	1.997(9)
	(Cu1–N3)	2.04(2)	(Cu2–N8)	2.00(2)	(Cu1–N3)	2.020(8)
	(Cu4–N11)	1.95(2)	(Cu3–N6)	2.02(2)		
	(Cu4–N12)	2.02(2)	(Cu3–N10)	1.96(2)		
S–S	(S1–S2)	2.088(7)	(S3–S4)	2.070(7)		
Bond Angles (deg)						
	1a		1b		2	
S1–Cu1–N1	138.5(4)		S4–Cu2–N5	108.3(5)	S1–Cu1–N1	131.6(3)
S1–Cu1–N2	91.5(5)		S4–Cu2–N8	135.6(5)	S1–Cu1–N2	91.9(3)
S1–Cu1–N3	110.1(5)		S4–Cu2–N9	91.4(5)	S1–Cu1–N3	111.5(3)
N1–Cu1–N2	98.8(6)		S3–Cu3–N6	109.4(5)	N1–Cu1–N2	102.5(4)
N2–Cu1–N3	100.8(6)		S3–Cu3–N7	91.3(4)	N2–Cu1–N3	99.5(4)
N3–Cu1–N1	107.2(6)		S3–Cu3–N10	134.7(5)	N3–Cu1–N1	111.2(3)
S2–Cu4–N4	91.7(5)		N5–Cu2–N8	111.6(7)		
S2–Cu4–N11	134.9(6)		N8–Cu2–N9	100.4(7)		
S2–Cu4–N12	108.3(5)		N9–Cu2–N5	99.6(6)		
N4–Cu4–N11	100.8(8)		N6–Cu3–N7	99.4(7)		
N11–Cu4–N12	111.9(8)		N7–Cu3–N10	100.9(8)		
N12–Cu4–N4	99.5(7)		N10–Cu3–N6	111.9(8)		
Dihedral Angles (deg)						
	1a		1b			
C15–S1–S2–C16		109.5(3)	C31–S3–S4–C54		103(1)	
Cu1–S1–S2–Cu4		–46.6(3)	Cu2–S4–S3–Cu3		–51.8(3)	

Interestingly, **1** has two independent structures, **1a** and **1b**, which chiefly differ in S–S bond distances, Cu(I)···Cu(I) separations, and C–S–S–C dihedral angles of the disulfide units. While the reaction of a Cu(II) salt with a thiol is well-known to lead to the redox decomposition Cu(II) + RSH → Cu(I) + RSSR,²³ this is the first example of the structurally characterized disulfide-bridged dicopper(I) complex synthesized through the redox reaction. The crystal structures of the cationic units in **1a** and **1b** are shown in Figure 2a,b. Selected bond lengths and bond angles are listed in Table 2.

The two Cu(I) ions are bridged by the disulfide units of the resultant ligands (Py₂SSPy₂) and separated by 4.035(3) Å in **1a** and 4.081(3) Å in **1b**. The disulfide S–S distances of 2.088(7) Å in **1a** and 2.070(7) Å in **1b** are longer than the value of 2.04 Å, a typical value observed in aliphatic disulfides.²⁴ The Cu–S distances of 2.228(6) and 2.246(6) Å in **1a** and 2.242(6) and 2.246(6) Å in **1b** are extremely short compared with the observed Cu–S distances of 2.28–2.40 Å in disulfide–copper(I) complexes.^{24a} The angles S1–Cu1–N1 and S2–Cu4–N11 in **1a** and S4–Cu2–N8 and S3–Cu3–N10 in **1b** are large, which would be ascribed to the intramolecular steric repulsion between the pyridine rings that are aligned face to face. The C15–S1–S2–C16 dihedral angle of 109.5(10)° in **1a** and the C31–S3–S4–C54 dihedral angle of 103(1)° in **1b** are different from those of aliphatic disulfides whose C–S–S–C dihedral angles are close to 90°. ^{24a} These structural features of the

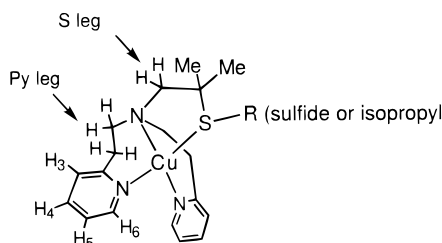
elongated disulfide S–S bond, the short Cu–S bond, and the C–S–S–C dihedral angle alteration from 90° would be associated with electron density delocalization of the Cu(I) ions to the sulfur 3p or 3d orbitals. Therefore, we can view complex **1** as an intermediate structure in the disulfide S–S bond formation by a catalytic oxidation of the thiol by the Cu(II) salt.

Complex **2** was crystallized in the space group *Pbca*. The crystal structure of the cation in **2** is shown in Figure 2c. As shown in Table 2, the Cu–S distance of 2.249(3) Å is shorter than that of 2.335(1) Å observed in the thioether–copper(II) complex [MeSPY₂]Cu(ClO₄)₂·CH₃CN synthesized by Réglier and co-workers.¹³ Recently, Rorabacher et al. also observed short Cu–S bond distances in [Cu^I(TMMEA)] (2.26(1) Å) and [Cu^I(TEMEA)] (2.262(6) Å).²² These Cu–S bond distances are elongated to 2.38(2) and 2.366(2) Å, respectively, when the Cu(I) centers are oxidized to the Cu(II) centers. The short Cu^I–SR₂ distance in **2** is on the short end from a survey of known thioether–copper(I) complex structures in the Cambridge database (*R* < 0.08).²² In the reduced form of PHM and DβM, the Cu–S distances were estimated to be 2.27 and 2.25 Å by spectroscopies,^{7,11b} and thus **2** has structural relevance to the reduced form of the copper enzymes.

Spectroscopic Properties. In Figure 3 we show the absorption properties of complexes **1**, **2**, and **3** and the disulfide Py₂SSPy₂ ligand. The ligand Py₂SSPy₂ was obtained by removing the copper ions from **1** with an NH₄OH solution. Complex **1** exhibits intense absorption bands at 263 nm ($\epsilon = 13\,600\text{ M}^{-1}\text{ cm}^{-1}$) and 300 nm ($\epsilon = 10\,900\text{ M}^{-1}\text{ cm}^{-1}$), as shown in Figure 3a. The intense 263 nm band is also shown by the disulfide Py₂SSPy₂ ligand, and thus this band would arise from a pyridine $\pi \rightarrow \pi^*$ chromophore or a disulfide chromo-

(23) Reaction of a Cu(II) salt with a thiol is known to lead to a redox decomposition [Cu(II) + RSH → Cu(I) + RSSR]: Mandal, S.; Das, G.; Singh, R.; Shukla, R.; Bharadwaj, P. K. *Coord. Chem. Rev.* **1997**, *160*, 191.

(24) (a) Warner, L. G.; Ottersen, T.; Seff, K. *Inorg. Chem.* **1974**, *13*, 2819; and references therein. (b) Boyd, D. B. *J. Am. Chem. Soc.* **1972**, *94*, 8799.

Table 3. ^1H NMR Data (Measured in CD_3CN at Room Temperature)


	chemical shift assignments, ppm (<i>J</i> , Hz)					
	pyr-H3	pyr-H4	pyr-H5	pyr-H6	CH_2 (S leg)	$-(\text{CH}_2)_2-$ (Py legs)
Py_2SSPy_2	7.19 (d, 7.8)	7.59 (td, 7.8)	7.11 (t, 6.2)	8.45 (d, 3.9)	2.60 (s)	3.00–2.88 (m)
1	7.36 (d, 7.8)	7.82 (td, 7.7)	7.24 (br)	8.07 (br)	2.78 (s)	2.88 (br), 2.69 (br)
$\Delta\delta(\mathbf{1} - \text{Py}_2\text{SSPy}_2)^a$	0.17	0.23	0.13	-0.38	0.18	nd ^b
$^i\text{PrSPy}_2$	7.22 (d, 8.1)	7.62 (td, 7.7)	7.13 (t, 6.3)	8.47 (d, 5.1)	2.61 (s)	3.04–2.89 (m)
2	7.39 (d, 8.1)	7.85 (td, 7.8)	7.36 (t, 6.5)	8.69 (d, 4.5)	2.70 (s)	2.93 (t, 4.8), 2.77 (t, 4.3)
$\Delta\delta(\mathbf{2} - ^i\text{PrSPy}_2)^a$	0.17	0.23	0.23	0.22	0.09	nd ^b

^a Coordination shift ($\Delta\delta$ (ppm) = $\delta(\text{complex}) - \delta(\text{ligand})$). ^b Not determined.

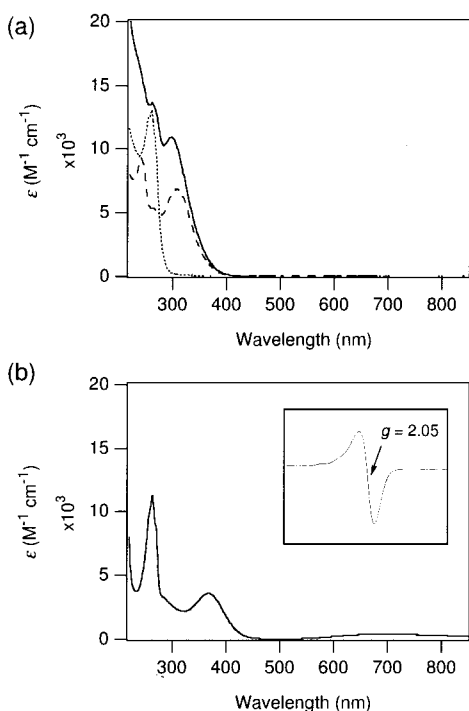
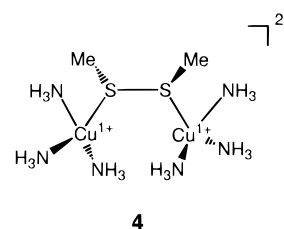


Figure 3. (a) UV–vis spectra of **1** (solid line), **2** (dashed line), and the disulfide ligand of Py_2SSPy_2 (dotted line). (b) UV–vis spectrum of **3**. Inset: EPR spectrum of **3**.

phore^{24b} rather than a $\text{Cu(I)} \rightarrow$ disulfide MLCT band.^{24a} However, a disulfide chromophore does not usually exhibit such a strong absorption.²⁴ Considering that complexes **2** and **3** (Figure 3b) also show intense bands at 243 nm ($\epsilon = 9200 \text{ M}^{-1} \text{ cm}^{-1}$) and 263 nm ($\epsilon = 11\,300 \text{ M}^{-1} \text{ cm}^{-1}$), respectively, these strong absorption features in the 240–260 nm region would be ascribed to pyridine chromophores.^{24a} The intense absorption band at 300 nm in **1** is not observed for the disulfide Py_2SSPy_2 ligand, suggesting that the band is a $\text{Cu(I)} \rightarrow$ disulfide MLCT band. This MLCT band in **1** is stronger than the absorption at 308 nm ($\epsilon = 6800 \text{ M}^{-1} \text{ cm}^{-1}$) in **2**, which would be ascribed to a $\text{Cu(I)} \rightarrow$ thioether MLCT band, reflecting the color of the complexes, yellow for **1** and pale yellow for **2**.

An EPR spectrum of **3** in CH_3CN solution at 77 K (Figure 3b inset) exhibits an isotropic signal at $g = 2.05$, indicating the copper center to be a divalent state. An absorption spectrum of

Chart 1

3 shows a thioether $\rightarrow \text{Cu(II)}$ LMCT band at 365 nm ($\epsilon = 3600 \text{ M}^{-1} \text{ cm}^{-1}$) and a d–d transition band at 685 nm ($\epsilon = 200 \text{ M}^{-1} \text{ cm}^{-1}$), a typical spectroscopic feature for Cu(II) –thioether complexes.

To elucidate the coordination environments in **1** and **2**, we measured ^1H NMR spectra of Py_2SSPy_2 , $^i\text{PrSPy}_2$, and complexes **1** and **2** in CD_3CN solutions, and assigned observed peaks, as listed in Table 3. We define the coordination shift ($\Delta\delta(\text{ppm}) = \delta(\text{complex}) - \delta(\text{ligand})$)²⁵ to describe changes in the electronic properties of the ligands by the coordinations. As for the methylene hydrogens of the Py legs in **1** and **2**, all are upfield-shifted; i.e., the negative values of the coordination shift indicate that the *tertiary* amino groups should coordinate as π -acceptors. On the other hand, the downfield-shifted coordination shifts are observed for the methylene hydrogens of the S legs, thereby indicating the significant σ -donation from the S-donors to the copper centers. A notable feature in the coordination shift is the significantly upfield-shifted and broadened signal of pyr-H6 in **1**, while other protons of the pyridine rings of **1** and **2** are all downfield-shifted. Thus, the pyridyl moieties in **1** would be stronger π -acceptors than those in **2**, and accordingly the electronic structure of the Cu(I) centers of **1** would be considerably different from that of **2** by the coordination of the ligands.

Molecular Orbital Analyses for the Disulfide–Dicopper(I) Complex. To gain deeper insights into the electronic properties of complex **1**, we performed extended Hückel calculations^{26,27} on the simplified model **4** (Chart 1). Bond distances and angles were averaged using the X-ray structural data to impose the C_2

(25) Kojima, T.; Amano, T.; Ishii, Y.; Ohba, M.; Okaue, Y.; Matsuda, Y. *Inorg. Chem.* **1998**, *37*, 4076.

(26) Extended Hückel calculations were carried out using YAeHMOP: Landrum, G., Cornell University, Ithaca, NY, 1995.

(27) (a) Hoffmann, R.; Lipscomb, W. N. *J. Chem. Phys.* **1962**, *36*, 2179; *37*, 2872. (b) Hoffmann, R. *J. Chem. Phys.* **1963**, *39*, 1397.

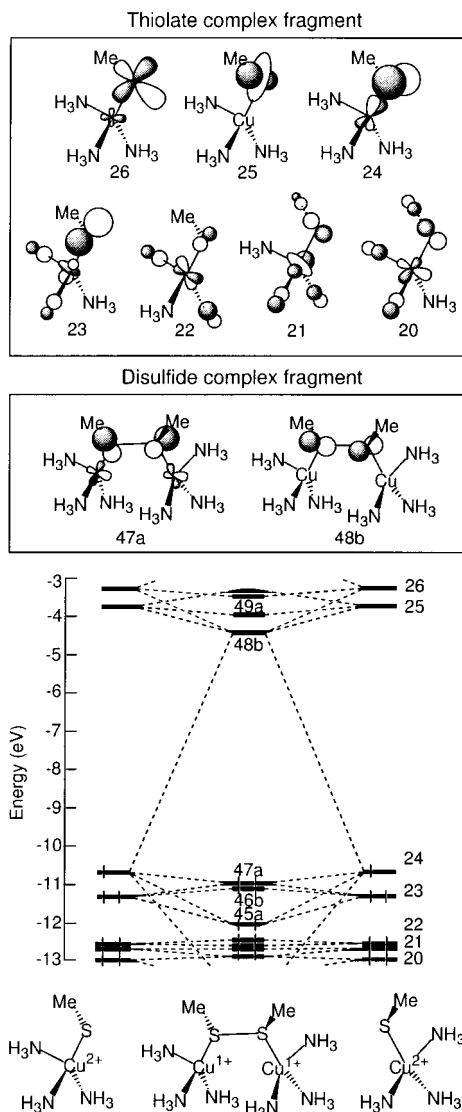


Figure 4. Orbital interaction diagram for **4**.

structure of **4**. The structural parameters and the extended Hückel parameters²⁸ used for this calculation are shown in the Appendix. To understand the governing orbital interactions,²⁹ we carried out fragment molecular orbital (FMO) analyses, partitioning **4** into two thiolate–copper(II) fragments. The bonding in **4** is then considered as shown in Figure 4. The HOMO (no. 24) at -10.69 eV of the thiolate–copper(II) fragment is the singly occupied orbital composed mainly of the sulfur p orbital and the copper d orbital. The two singly occupied orbitals strongly interact to make the disulfide bond in **4** through the σ -type interactions of the sulfur p orbitals, and the antibonding interaction constitutes the significantly destabilized LUMO (no. 48b) at -4.33 eV.

For a closer inspection of the bonding and the antibonding interactions between the two thiolate units, we carried out MOOP (molecular orbital overlap population) analyses³⁰ (Figure 5). The MOOP plot for the S–S bond shows graphically the contribution of various MOs to the Mulliken overlap population.

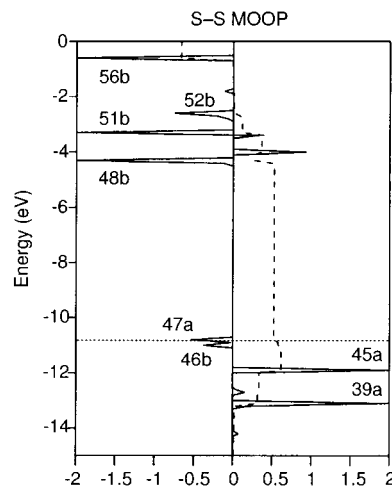


Figure 5. MOOP analysis for the S–S bond of **4**. The dotted line indicates the HOMO level and the dashed line running up the integration of bonding and antibonding interactions.

In these, the bonding contributions are plotted to the right and the antibonding ones to the left. The dotted line shows the HOMO levels; the dashed line running up indicates the integrations up to the indicated energy of all bonding and antibonding contributions. It is of great use to look at the MOOP plot together with the FMO analysis in Figure 4. The HOMO (no. 47a) is slightly antibonding between the S atoms of the disulfide. There are four main S–S antibonding orbitals, i.e., no. 48b at -4.33 eV, no. 51b at -3.31 eV, no. 52b at -2.74 eV, and no. 56b at -0.59 eV. Since these strongly antibonding orbitals are unoccupied, the net overlap population at the HOMO level is positive. To break the S–S bond of the disulfide, the no. 52b orbital at -2.74 eV, at which level the integration of the overlap population between the S atoms indicates almost zero, must be filled with electrons, thereby permitting the stable S–S bond formation.

Catalytic Oxidation of Hydrocarbons. Our interests have been focused on the catalytic functions of complexes **1–3**. Studies on the oxidation of alkanes by copper complexes in the presence of H_2O_2 ^{31–33} are limited compared with extensive investigations on iron complexes/ H_2O_2 catalysts.^{34–36} As a comparison we also employed tBuOOH as an oxygen source. Results of catalytic oxidations of hydrocarbons are listed in Table 4.

Relatively low yields of products were obtained, due to ligand decomposition by self-oxidation, which may be carried out by

(28) Alvarez, S., Universitat de Barcelona, Barcelona, 1993.

(29) Albright, T. A.; Burdett, J. K.; Whangbo, M.-H. *Orbital Interactions in Chemistry*; Wiley: New York, 1985.

(30) MOOP was introduced by D. M. Prosperio and C. Mealli in CACAO (a package of programs for extended Hückel molecular orbital analysis).

(31) Okuno, T.; Ohba, S.; Nishida, Y. *Polyhedron* **1997**, *16*, 3765.

(32) Sobkowiak, A.; Quin, A.; Liu, X.; Llobet, A.; Sawyer, D. T. *J. Am. Chem. Soc.* **1993**, *115*, 609.

(33) Barton, D. H. R.; Beviere, S. D.; Chavasiri, W.; Chsuhai, E.; Doller, D. *Tetrahedron* **1992**, *48*, 2895.

(34) (a) Barton, D. H. R.; Doller, D. *Acc. Chem. Res.* **1992**, *25*, 504. (b) Meunier, B. *Chem. Rev.* **1992**, *92*, 1211. (c) Valentine, J. S.; Nam, W.; Ho, R. Y. N. In *The Activation of Dioxygen and Homogeneous Catalytic Oxidation*; Barton, D. H. R., Martell, A. E., Sawyer, D. T., Eds.; Plenum: New York, 1993. (d) Sawyer, D. T.; Sobkowiak, A.; Matsushita, T. *Acc. Chem. Res.* **1996**, *29*, 409.

(35) (a) Fish, R. H.; Konings, M. S.; Oberhausen, K. J.; Fong, R. H.; Yu, W. M.; Christou, G.; Vincent, J. B.; Coggins, D. K.; Buchanan, R. M. *Inorg. Chem.* **1991**, *30*, 3002. (b) Ménage, S.; Vincent, J.-M.; Lambeaux, C.; Fontecave, M. *J. Mol. Catal., A* **1996**, *113*, 61. (c) Nguyen, C.; Guajardo, R. J.; Mascharak, P. K. *Inorg. Chem.* **1996**, *35*, 6273.

(36) (a) Lubben, M.; Meetsma, A.; Wilkinson, E. C.; Feringa, B.; Que, L., Jr. *Angew. Chem., Int. Ed. Engl.* **1995**, *34*, 1512. (b) Kim, J.; Harrison, R. G.; Kim, C.; Que, L., Jr. *J. Am. Chem. Soc.* **1996**, *118*, 4373. (c) Kim, C.; Chen, J. K.; Kim, J.; Que, L., Jr. *J. Am. Chem. Soc.* **1997**, *119*, 5964. (c) Chen, K.; Que, L., Jr. *Chem. Commun.* **1999**, 1375.

Table 4. Oxidation of Hydrocarbons by **1**–**3**/Peroxides^a

Oxidation of Cyclohexane					
complex	peroxide	gas	product yield (%) ^b		selectivity alcohol/ketone
			cyclohexanol	cyclohexanone	
1	H ₂ O ₂	Ar	41	18	2.2
	H ₂ O ₂	O ₂	44	30	1.5
	^t BuOOH	Ar	12	14	0.9
2	H ₂ O ₂	Ar	44	19	2.3
	^t BuOOH	Ar	34	24	1.4
3	H ₂ O ₂	Ar	17	13	1.3
	^t BuOOH	Ar	trace	6	0

Oxidation of Cyclohexene					
complex	peroxide	gas	product yield (%) ^b		
			cyclohexene oxide	2-cyclohexen-1-ol	2-cyclohexen-1-one
1	H ₂ O ₂	Ar	9	24	24
	H ₂ O ₂	O ₂	3	10	23
	^t BuOOH	Ar	nd	14	31
2	H ₂ O ₂	Ar	nd	19	19
	^t BuOOH	Ar	nd	22	39
3	H ₂ O ₂	Ar	nd	13	13
	^t BuOOH	Ar	trace	6	6

^a Reaction conditions: 0.5 mmol of a peroxide was slowly added to a stirred 5 mL CH₃CN solution containing the complex (50 μmol) and 1 mmol of substrate. The reaction mixture was stirred for 30 min at 25 °C. The products listed were analyzed and quantified by GC using PhCl as an internal standard. ^b Moles of product/moles of complex.

the sulfoxidation of the disulfide moiety.³⁸ Under Ar conditions, the selective oxidation of cyclohexane to cyclohexanol with an alcohol/ketone ratio of 2.2 and 2.3 was achieved by the **1**/H₂O₂ and **2**/H₂O₂ combinations, respectively. For the **1**/H₂O₂ combination the alcohol/ketone ratio of 2.2 was reproduced three times with an error of ±0.2. Furthermore, this ratio was not significantly changed with an alcohol/ketone ratio of 1.5 when the reaction was carried out by **1**/H₂O₂ under O₂ conditions. A combination of a metal complex with a peroxide is often considered to generate a hydroxyl or an alkoxy radical that initiates a radical chain autoxidation reaction,^{36b,c,37} and in this reaction alkane is oxidized typically with an alcohol/ketone ratio of about 1. We thus think that a metal-based oxidant may be formed by the **1**/H₂O₂ and **2**/H₂O₂ combinations. To consider the nature of the metal-based oxidant, ^tBuOOH was used in place of H₂O₂. The **1**/^tBuOOH and **2**/^tBuOOH combinations, on the contrary, oxidized cyclohexane to cyclohexanol and cyclohexanone with an alcohol/ketone ratio of about 1, thereby indicating the predominance of an alkoxy radical mechanism. Oxidation reactions showed by **3**/peroxides were all radical-type autoxidations, and in every run we observed the products of benzyl alcohol and phenylethyl alcohol that might be generated by the oxidation of the phenylethyl moiety of the ligand.

A metal-based oxidant is considered to be formed in both the **1**/H₂O₂ and **2**/H₂O₂ combinations, while interesting differences in the reactivity for cyclohexene were observed. While the **1**/H₂O₂ combination catalyzed the epoxidation of cyclohexene under Ar conditions, the **2**/H₂O₂ system did not. Thus, in the **1**/H₂O₂ combination a metal-based oxidant different from that for the hydroxylation may be concerned with the epoxidation. The observed oxidation selectivity by **1**/H₂O₂ for the

epoxidation (E) versus the allylic oxidation (A) with an E/A ratio of 0.2 (observed ratio error ±0.02) is much higher than the E/A ratio of 0.3 shown by Kitajima's μ-peroxo-dicopper(II) complex.³⁹ In the μ-peroxo-dicopper(II) complex, a Cu(II)–O• radical generated by the O–O homolysis of the peroxide has been proposed to be responsible for the formation of cyclohexyl radical to yield major products of 2-cyclohexen-1-ol and 2-cyclohexen-1-one. Therefore, in our **1**/H₂O₂ system, a metal-based oxidant that is different from the Cu(II)–O• species is considered to participate in the olefin epoxidation. The **1**/^tBuOOH combination did not catalyze the epoxidation in remarkable contrast to the Cu^I(bpy)₂⁺/^tBuOOH system of Sawyer³² that catalyzes selective epoxidation of cyclohexene. As reported previously,¹⁴ the oxidative coupling of two 2,6-di-*tert*-butylphenols into 3,3',5,5'-tetra-*tert*-butyl-4,4'-diphenylquinone, which is effectively catalyzed by the μ-peroxo-dicopper(II) complex,^{39a} did not take place in our complex well, while a number of minor products that might be generated by a free radical type reaction initiated by phenoxy radical were observed. DβM was also demonstrated to catalyze not only the hydroxylation of the benzylic position of dopamine but also the activation of the O–H bonds of phenolic hydroxyl groups by an H• abstraction^{6b} and olefin epoxidations,⁸ and thus the oxidation reactions showed by the **1**/H₂O₂ combination could have relevance to the enzymatic oxygenation.

A Hydroperoxo–Dicopper(II) Intermediate. As previously reported,¹⁴ in the absence of a substrate hydrocarbon, the reaction of **1** with a 6-fold excess of H₂O₂ in a CH₃CN solution at –5 °C for 10 min yielded a dark green intermediate. At room temperature, the dark green color disappears within 10 s. The dark green intermediate shows absorption maxima at 295 nm (ε = 7700 M^{–1} cm^{–1}), 325 nm (sh) (ε = 6414 M^{–1} cm^{–1}), and 670 nm (br) (ε = 30 M^{–1} cm^{–1}). The EPR spectrum of a CH₃CN solution at 77 K exhibited monomeric decomposition derived signals at *g* ≈ 2 and a half-field transition of Δ*M_s* = ± 2,^{17,40} identifying the intermediate to be a dinuclear copper(II) complex (Figure 6a).

The resonance Raman spectra of the dark green intermediate in a CH₃CN solution measured at –25 °C (laser excitation wavelength 325 nm) revealed resonance-enhanced Raman features in the region of 800–850 cm^{–1}, which were fitted by two Gaussian functions to lead to the two peaks at 822 and 836 cm^{–1} (Figure 6b).^{41a} The bands were not observed before H₂O₂ was added to a CH₃CN solution containing **1**. Furthermore, the two peaks that appeared by adding H₂O₂ to **1**/CH₃CN at low-temperature disappeared by raising the temperature of the cold CH₃CN solution of the dark green intermediate to room

(37) (a) Sheldon, R. A.; Kochi, J. K. *Metal-Catalyzed Oxidations of Organic Compounds*; Academic: New York, 1981. (b) Kochi, J. K. *Tetrahedron* **1962**, *18*, 483.

(38) Yamauchi, O.; Seki, H. *Chem. Lett.* **1982**, 1241.

(39) (a) Kitajima, N.; Koda, T.; Iwata, Y.; Moro-oka, Y. *J. Am. Chem. Soc.* **1990**, *112*, 8833. (b) Kitajima, N.; Fujisawa, K.; Fujimoto, C.; Moro-oka, Y.; Hashimoto, S.; Kitagawa, T.; Toriumi, K.; Tatsumi, K.; Nakamura, A. *J. Am. Chem. Soc.* **1992**, *114*, 1277.

(40) (a) Boas, J. F.; Pilbrow, J. R. *J. Chem. Soc. A*, **1969**, 572. (b) Wilcox, D. E.; Long J. R.; Solomon, E. I. *J. Am. Chem. Soc.* **1984**, *106*, 2186.

(41) (a) While from the spectra in Figure 6b the reader may think that the broad peak cannot be divided into two bands, we observed the alteration of the intensity of the two peaks dependent on the reaction conditions, which cannot be controlled yet. Thus, we think that two bands are included in the broad band. (b) The concentration of H₂¹⁸O₂ used in this study was 500 mM, and such a solution froze rapidly when introduced to CH₃CN solution containing **1** at –20 °C. This prevents the formation of **1**(OOH) in good yield, resulting in the low S/N ratio for the ¹⁸O₂H spectrum. The appearance of the 822 and 836 cm^{–1} bands in the ¹⁸O₂H spectrum is due to the contamination of H₂¹⁶O₂ in our prepared aqueous H₂¹⁸O₂. See the Experimental Section. (c) We could not observe the band of a Cu–O stretching mode reproducibly. Such a stretching mode for a Cu–OOH species would show a weak signal as reported in ref 44d, but our low S/N ratio spectra seem to be unable to delineate weak bands.

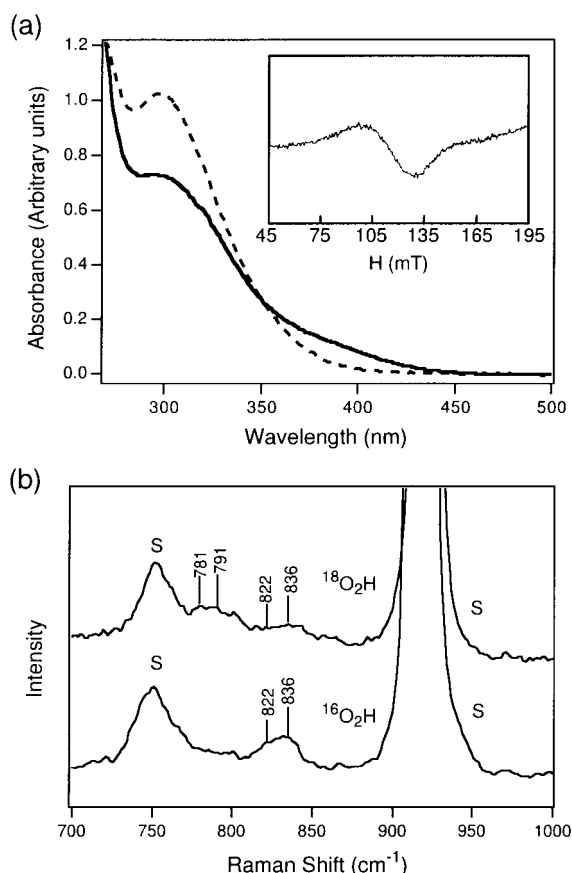


Figure 6. (a) Electronic absorption spectra of **1** (dashed line) and **1(OOH)** (solid line) in CH_3CN at 0°C . Inset: EPR spectrum of **1(OOH)** in the half-field transition region (77 K, microwave frequency 9.09 GHz, modulation 0.63 mT, microwave power 0.4 mW). (b) Resonance Raman spectra of **1(OOH)** in CH_3CN solution at -25°C . The spectrum was obtained with 325 nm laser excitation. Solvent bands are marked with an "s".

temperature, and thus the peaks would be ascribed to the feature of the dark green intermediate. The two peaks shifted to lower frequencies upon introduction of $\text{H}_2^{18}\text{O}_2$ with peak features at 781 and 791 cm^{-1} .^{41b} These vibrational features are in the range characteristic for the $\nu(\text{O}-\text{O})$ band of peroxide species. However, the absence of intense electronic absorption features in the 500–600 nm region,^{42,44b} which are associated with the electric dipole allowed peroxide(π^*)-to-copper CT bands, leads us to rule out a possibility for the formation of the *trans- μ -1,2* binding mode of peroxo species. The Raman bands at 822 and 836 cm^{-1} are close to the $\nu(\text{O}-\text{O})$ band at 856 cm^{-1} observed in the structurally characterized hydroperoxo-copper(II) complex of $[\text{Cu}(\text{bppa})(\text{OOH}^-)](\text{ClO}_4)$,⁴³ and thus the spectrum in Figure 6b may be suggestive of the formation of a hydroperoxo-copper species of **1(OOH)**.^{41c} The absorption features in

Table 5. Reported Resonance Raman Features of Copper- and Iron-Peroxo Complexes

complex	$\nu(\text{O}-\text{O})$ (cm^{-1})	ref
$[\text{Cu}_2(\text{Py}_2\text{SSPy}_2)(\text{OOH})_2]^{2-x+}$	822, 836	this work
$[\text{Cu}(\text{bppa})(\text{OOH})]^{1+}$	856	43
$[\text{Cu}_2(\text{UN}-\text{O}-)(\text{OOH})]^{2+}$	892	44d
$[\text{Cu}(\text{HB}(3,5\text{-Pr}_2\text{pz}_3)_2)(\text{O}_2)]$	741	39b
$[\{\text{Cu}(\text{TMPA})\}_2(\text{O}_2)]^{2+}$	832	44b
$[\text{Fe}(\text{TPA})(\text{OOH})]^{2+}$	789	45
oxyhemerythrin $[\text{Fe}(\eta^1\text{-OOH})]^{2+}$	844	46

Figure 6a can be attributed to a hydroperoxo-to-Cu CT transition.^{43,44a,c,d} However, due to the overlap of the strong CT bands, which may be ascribed to a sulfide-to-Cu CT band and/or a sulfide absorption, the CT band region is rather broad for exact assignment. The two $^{16}\text{O}_2$ bands at 822 and 836 cm^{-1} shifted into the two bands at 781 and 791 cm^{-1} by the $^{18}\text{O}_2$ substitution, with a frequency isotope ratio of $\nu(^{16}\text{O}_2)/\nu(^{18}\text{O}_2) = 1.052$ and 1.056 ($\Delta\nu = 41$ and 45 cm^{-1}), respectively. This matches the frequency ratio expected for ^{18}O -isotope replacement of an O–OH harmonic oscillator of 1.059 ($\Delta\nu = 49$ cm^{-1}),^{44d} implying that the O–O frequency in **1(OOH)** reflects the intrinsic stiffness of the O–O bond. The frequency shifts of the two bands tell us that they can be derived from two Cu–OOH species rather than the Fermi doublet.^{44d} It is also possible to consider that the two Raman features should result from the two independent structures of **1** determined by the X-ray analyses, while whether such a significant difference in the O–O bond activation comes from the nearly identical structures of **1a** and **1b** that should remain almost unchanged even in the oxidized forms is questionable.

For comparison, we show reported Raman shifts for the $\nu(\text{O}-\text{O})$ band that derived from iron- and copper-peroxo compounds^{39b,43–46} in Table 5. The 822 and 836 cm^{-1} O–O stretching frequencies of **1(OOH)** are lower than that observed for other hydroperoxo-copper complex^{43,44d} and comparable to 832 cm^{-1} observed in a *trans- μ* -peroxo complex of $[\{\text{Cu}(\text{TMPA})\}_2(\text{O}_2)]^{2+}$.^{44b} The low frequencies are suggestive of a significant weakening of the O–O bonds in our complex. In fact, **1(OOH)** converts a relatively inert hydrocarbon cyclohexane to cyclohexanol selectively, while other reported hydroperoxo-copper species^{43,44d} do not catalyze it. The significant weakening of the O–O bond could be associated with significant electron delocalization from the soft donor of the disulfide to the hydroperoxo moiety.

Given that the two bands are localized on the O–O stretching, an O–OH harmonic vibrational model gives O–O force constants of $k = 3.3$ $\text{mdyn}/\text{\AA}$ for the 822 cm^{-1} band and $k = 3.4$ $\text{mdyn}/\text{\AA}$ for the 836 cm^{-1} band. Because a Cu–O stretching frequency and other bending modes are not observed for our Cu–OOH complex, we cannot investigate in detail the vibrational feature of the Cu–OOH unit. Solomon et al. determined an O–O force constant of $k = 3.7$ $\text{mdyn}/\text{\AA}$ for a Cu–OOH complex using a Urey–Bradley force field,^{44d} in which the CuOO and OOH bending frequencies were varied over the range observed for analogous molecules. They reported that varying the OOH or CuOO bending frequencies does not greatly increase the contributions of the Cu–O symmetric stretch and the OOH bend internally coordinates to the O–O stretching mode and thus does not strongly affect the calculated O–O force constant.

- (42) (a) Shin, W.; Sundaram, U. M.; Cole, J. L.; Zhang, H. H.; Hedman, B.; Hodgson, K. O.; Solomon, E. I. *J. Am. Chem. Soc.* **1996**, *118*, 3202. (b) Sundaram, U. M.; Zhang, H. H.; Hedman, B.; Hodgson, K. O.; Solomon, E. I. *J. Am. Chem. Soc.* **1997**, *119*, 12525.
 (43) Wada, A.; Harata, M.; Hasegawa, K.; Jitsukawa, K.; Masuda, H.; Mukai, M.; Kitagawa, T.; Einaga, H. *Angew. Chem., Int. Ed. Engl.* **1998**, *37*, 798.
 (44) (a) Karlin, K. D.; Ghosh, P.; Cruse, R. W.; Farooq, A.; Gultneh, Y.; Jacobson, R. R.; Blackburn, N. J.; Strange, R. W.; Zubieta, J. *J. Am. Chem. Soc.* **1988**, *110*, 6769. (b) Baldwin, M. J.; Ross, P. K.; Pate, J. E.; Tyeklár, Z.; Karlin, K. D.; Solomon, E. I. *J. Am. Chem. Soc.* **1991**, *113*, 8671. (c) Tahir, R. R.; Murthy, N. N.; Karlin, K. D.; Blackburn, N. J.; Shaikh, S. N.; Zubieta, J. *Inorg. Chem.* **1992**, *31*, 3001. (d) Root, D. E.; Mahroof-Tahir, M.; Karlin, K. D.; Solomon, E. I. *Inorg. Chem.* **1998**, *37*, 4838.

- (45) Ho, R. Y. N.; Roelfes, G.; Feringa, B. L.; Que, L., Jr. *J. Am. Chem. Soc.* **1999**, *121*, 264.
 (46) (a) Kurtz, D. M., Jr.; Shriver, D. F.; Klotz, I. M. *J. Am. Chem. Soc.* **1976**, *98*, 5033. (b) Shiemke, A. K.; Loehr, T. M.; Sonders-Loehr, J. *J. Am. Chem. Soc.* **1984**, *106*, 4951.

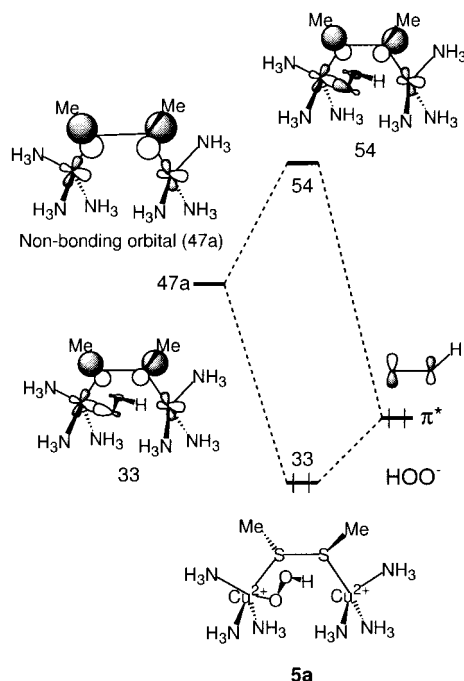
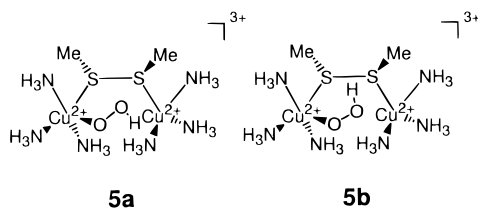


Figure 7. Orbital interaction for the Cu–OOH bond formation.

Chart 2



Indeed by assuming a simple O–OH vibration, the 889 cm^{-1} mode gives an O–O force constant of 3.8, being slightly larger than the value from the Urey–Bradley model. Thus, a simple O–OH stretching model would give reliable information about the stiffness of the O–O bond in a Cu–OOH species. The force constants of 3.3 and 3.4 of our model are larger than that of 3.1 for the end-on dicopper–peroxo complex, the O–O stretching frequency of which is 832 cm^{-1} ,^{44b} indicating that while these stretching frequencies are almost equal, the O–O bond is slightly harder in our Cu–OOH complex than in the end-on dicopper–peroxo complex.

Molecular Orbital Analyses for the Hydroperoxo–Dicopper(II) Intermediate. To investigate the electronic properties of the observed hydroperoxo–dicopper(II) complex, extended Hückel calculations^{26,27} on model hydroperoxo–dicopper(II) complexes were performed. For the hydroperoxo-bound disulfide-bridged dicopper(II) complex, we have built two models, **5a** and **5b** (Chart 2), that have a *trans*- and a *cis*-Cu–OOH moiety, respectively.

Let us first look at an orbital interaction which is essential for this Cu(II)–OOH bond formation in **5a** (Figure 7). For this purpose we partitioned the hydroperoxo–dicopper(II) complex into one fragment composed of the dicopper(II) active site model and another composed of the HOO^- anion. Although the position of the terminal OH group of the Cu–OOH moiety in **5a** can be altered by rotating it around the Cu–OOH axis, for this FMO analysis we set the dihedral angle of S–Cu–O–O to be 70° by rotating the OH group to the anticlockwise direction when the axis is seen from O to Cu. As we will discuss later, this is one of the stable conformations of the Cu–OOH moieties.

Table 6. Structural Parameters for Models **4**, **5a**, and **5b**^a

distance (Å)	angle (deg)				
Cu–S	2.24	Cu–S–S	110.1	Cu–S–S–Cu	46.6
S–S	2.09	S–Cu–N1	138.0	C–S–S–Cu	142.9
Cu–N	2.06	S–Cu–N2	112.5	Cu–O–O–H	180 (0) ^d
C–S	1.89	S–Cu–N3	112.5		
Cu–O ^c	1.89	Cu–O–O ^c	114.5		
O–O ^c	1.46				

^a The C–H and N–H distances are set to be 0.95 Å. ^b Dihedral angle. ^c For **5a** and **5b**. Taken from ref 43. ^d For **5a** (**5b**).

The other structural parameters for **5a** are listed in the Appendix (Table 6). When the Cu(I) centers of **4** are oxidized to the divalent state, the no. 47a orbital at –10.83 eV, shown in Figure 4, becomes the LUMO that involves the nonbonding copper d orbital. Since this nonbonding copper d orbital can make the important two-electron two-orbital interactions^{29,48} with one of the lone-pair orbitals (π^*) of the HOO^- anion, the Cu(II)–OOH bond is stabilized. On the contrary, from the perturbational molecular orbital theory,²⁹ the Cu(I) centers in **4** cannot make stable bonding with the HOO^- anion because the nonbonding copper d orbital of **4** is very high-lying compared with the π^* orbital of the HOO^- anion. Recent SCF–X α –SW calculations^{44d} on the $(\text{NH}_3)_3\text{Cu}$ –OOH model showed that the main copper–oxygen interaction between the Cu $d_{x^2-y^2}$ orbital and the π^* orbital of the HOO^- anion makes the bonding and antibonding interactions separated by 3.2 eV, and the antibonding orbital is singly occupied. Our extended Hückel calculation for **5a** indicates the energy separation between the bonding (no. 33) and the antibonding (no. 54) interactions to be 4.9 eV, and the strong antibonding orbital is unoccupied. Although we cannot directly compare our extended Hückel calculation with the SCF–X α –SW calculations,^{44d} the Cu–OOH bond in **5a** can be reasonably formed with this large binding energy.

Let us next look at an MOOP analysis for the hydroperoxo complex **5a**, shown in Figure 8. There are two main Cu–O antibonding orbitals, i.e., no. 45 at –13.58 eV and no. 54 at –10.13 eV. The no. 54 orbital is derived from the π^* orbital of the HOO^- anion and the nonbonding copper $d_{x^2-y^2}$ orbital, as shown in Figure 7. The strongly antibonding no. 54 orbital is unoccupied, so the net overlap population at the HOMO is positive. The no. 54 orbital at –10.13 eV is only 0.7 eV different from the HOMO at –10.82 eV, and thus this Cu–OOH bond would be easily cleaved by thermal and photochemical excitations.

As a next step, we considered the conformation of the Cu–OOH moiety. We rotated the Cu–OOH unit along the Cu–O axis in **5a** and **5b** and calculated the total energies of the complexes (Figure 9). The thick and thin lines in Figure 9 represent the changes in the total energies of **5a** and **5b**, respectively, as a function of the S–Cu–O–OH dihedral angle

(47) (a) *Cytochrome P450: Structure, Mechanism, and Biochemistry*, 2nd ed.; Ortiz de Montellano, P. R., Ed.; Plenum: New York, 1995. (b) Sono, M.; Roach, M. P.; Coulter, E. D.; Dawson, J. H. *Chem. Rev.* **1996**, *96*, 2842.

(48) (a) Yoshizawa, K.; Yamabe, T.; Hoffmann, R. *New J. Chem.* **1997**, *21*, 151. (b) Yoshizawa, K.; Ohta, T.; Yamabe, T. *Bull. Chem. Soc. Jpn.* **1997**, *70*, 1911. (c) Yoshizawa, K.; Ohta, T.; Yamabe, T.; Hoffman, R. *J. Am. Chem. Soc.* **1997**, *119*, 12311.

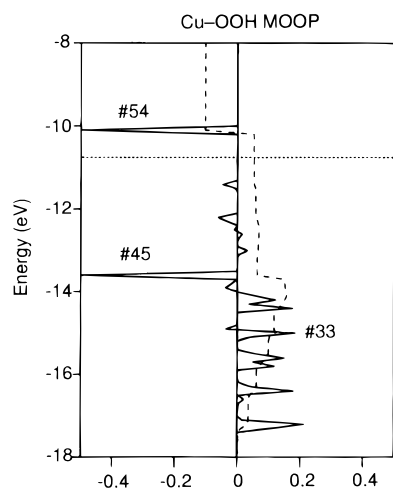


Figure 8. MOOP analysis for the Cu-OOH bond of **5a**.

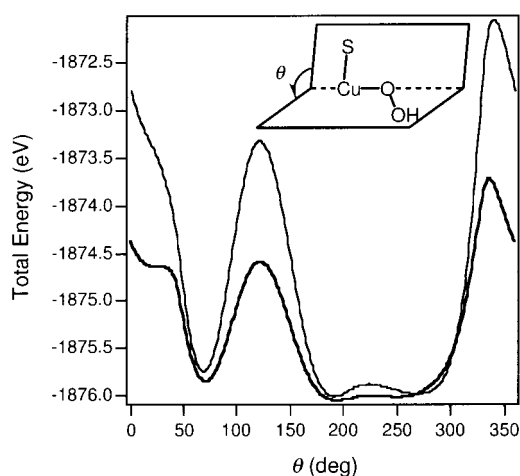


Figure 9. Total energy diagrams along the S-Cu-O-OH dihedral angle (θ) alteration for **5a** (thick line) and **5b** (thin line).

(Figure 9 inset). When the S, Cu, and O atoms and the OH group are in the same plane, we set the dihedral angle to be 0° . Both **5a** and **5b** have nearly equal potential minimum energies at $\theta = 73^\circ$, 193° , and 265° , and the differences in the total energies of **5a** and **5b** are negligibly small. The potential barriers in Figure 9 are a result of the steric repulsion between the OOH moiety and the ligands. In the θ range of 180 – 284° , the total energy surfaces have very flat curvatures, and thus in this range any conformation of the Cu-OOH moieties is possible.

Mechanistic Considerations. The observed catalytic functions and the weakened CuO-OH bond shown by **1(OOH)** are intriguing, considering the possible relevance to the enzymatic activation of the O-O bond and hydrocarbons. The Cu-OOH species of **1(OOH)** has Cu(II) centers, so that an initial key reaction for the generation of **1(OOH)** is the oxidation of the Cu(I) centers by H_2O_2 . In the oxidation a hydroxyl radical would be formed,^{37b} which can also play a role in the oxidation of hydrocarbon substrates with reduction of the alcohol/ketone and epoxidation/allylic oxidation ratios. At 25°C intermediate **1(OOH)** is less stable than a purple Fe^{III} -OOH intermediate,^{36a} which was reported to be able to oxidize cyclohexane selectively to cyclohexanol in high efficiency. Thus, the dark green intermediate **1(OOH)** is reasonably proposed to be kinetically competent in the oxidation of hydrocarbon substrates.

The two resonance Raman features of the $\nu(\text{O}-\text{O})$ bands at 822 and 836 cm^{-1} suggest the presence of two kinds of Cu-OOH species in **1(OOH)**, and from the 14 cm^{-1} differences in

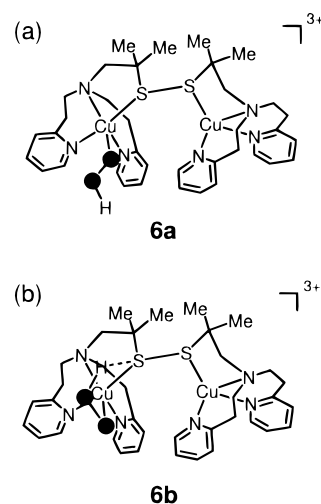
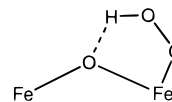


Figure 10. Proposed structures for **1(OOH)**: (a) *trans*- and (b) *cis*-Cu-OOH moieties.

Chart 3



the vibrational data, we expect significant differences in the conformational features for the two Cu-OOH species. In the dinuclear iron site of oxyhemerythrin, the peroxide is known to bind to the iron center in the η^1 manner with making of the hydrogen bond with the bridging oxo group (Chart 3).^{46,49} The resonance Raman feature of 844 cm^{-1} for the O-O bond denotes the strong O-O bond compared with that of observed peroxy-iron species.

By analogy to oxyhemerythrin, in our model the nucleophilic S atom of the disulfide moiety in the vicinity of the Cu center may form a hydrogen bond with the terminal H atom of the Cu-OOH moiety. Combined with the result of the extended Hückel calculation for **5a** and **5b** in Figure 9, we propose two possible structures for **1(OOH)**, as shown in Figure 10. Complex **6a** has a *trans*-Cu-OOH moiety with the S-Cu-O-OH dihedral angle in the range of 180 – 284° , as shown in Figure 9. Complex **6b** has a *cis*-Cu-OOH moiety with the terminal H atom making a hydrogen bond with the S atom of the disulfide moiety. The S-Cu-O-OH dihedral angle in **6b** is about 70° from the extended Hückel calculations for **5b** (Figure 9). From the conformational analyses of **5a** and **5b** in Figure 9, we expect that the *cis*-Cu-OOH moiety of **6b** should be less stable than the *trans*-Cu-OOH moiety of **6a**.

The proposed hydrogen bonding may stabilize **6b** more than **6a**. Nishida et al. previously proposed such a hydrogen bond between the H atom of the hydroperoxide coordinating to the Cu(II) center of $[\text{Cu}(\text{bdpg})\text{Cl}]\text{Cl}$ and the O atom of the amide moiety of the ligand,³¹ although they did not characterize the O-O bond of the hydroperoxide species from vibrational analyses. The recent SCF-X α -SW calculations^{44d} on a hydroperoxy-copper(II) complex clarified the effect of protonation of the terminal O atom of the peroxy-copper(II) species on the O-O bond strength; the proton stabilizes the orbitals on the oxygen to which it is bound, and both the intraperoxy π -bonding and π -antibonding interactions are disrupted by the protonation, the net result being an increase in the O-O bond

(49) (a) Brunold, T. C.; Solomon, E. I. *J. Am. Chem. Soc.* **1999**, *121*, 8277.
(b) Brunold, T. C.; Solomon, E. I. *J. Am. Chem. Soc.* **1999**, *121*, 8288.

strength.^{44d} Therefore, the hydrogen bonding in **6b**, by which the CuOO–H bond is weakened, would increase the activation of the CuO–OH bond, and consequently the Raman feature observed in **1**(OOH) is thought to show two bands. We thus think that the Raman features of 822 and 836 cm⁻¹ may be ascribed to the O–O vibrations in **6b** and **6a**, respectively.

Oxyhemerythrin has a hydrogen-bonded Fe(III)–OOH species as discussed above and shows a 4 cm⁻¹ increase in the O–O stretching frequency when D replaces H in a coordinated hydroperoxide.^{46b} This phenomenon cannot be simply explained by a change in mass. Similarly the $\nu(\text{O–O})$ of D₂O₂ shows no mass effect.⁵⁰ For cobalt-substituted myoglobin and hemoglobin, in which the bound dioxygen is believed to be hydrogen bonded to the distal histidine, the $\nu(\text{O–O})$ shifts from 1124 to 1136 cm⁻¹ for oxyCoMb and from 1133 to 1138 cm⁻¹ for oxyCoHb upon deuteration.⁵¹ Thus, it is of future interest to investigate the nature of the O–O stretching of **1**(OOD).

We cannot determine so far whether the observed reactivity of the **1**/H₂O₂ combination is concerned with the Cu–OOH species or a more activated Cu(II)–O• (Cu(III)=O) species that can be formed by the homolysis or heterolysis of the CuO–OH bond. However, the increased selectivity of the epoxidation versus the allylic oxidation of cyclohexene (E/A) by the **1**/H₂O₂ system (E/A = 0.18) compared with Kitajima's μ -peroxydicopper(II) complex (E/A = 0.03)^{39a} is one of the distinctive features that may offer clues to understanding the oxidation mechanism performed by **1**/H₂O₂. In Kitajima's complex^{39a} the O–O bond of the peroxy is proposed to be cleaved homolytically to yield the Cu(II)–O• species, which attacks the allylic position of cyclohexene in a radical-type reaction. Therefore, if we assume that the CuO–OH bond in **1**(OOH) is cleaved before substrate oxidations, the heterolytic cleavage mechanism of the hydroperoxy O–O bond by the single-electron-transfer mechanism¹³ of the disulfide moiety may be more predominant to yield an S⁺Cu(II)–O• or an S⁺Cu(III)=O species. However, since the S⁺Cu(II)–O• species will oxidize selectively the allylic position of cyclohexene in the radical manner with reduction of the E/A ratio, in our model the S⁺Cu(III)=O species may be sustained with the aid of the donor ability of the S-donor ligand.

An alternative mechanistic option is that the observed Cu–OOH species is the actual oxidant for the epoxidation and the hydroxylation, although spectroscopically characterized Cu–OOH^{43,44d} species are weak oxidants for the hydroxylation of cyclohexane and the epoxidation of olefins. In our model, however, the O–O bond is significantly activated, and thus it is also possible to consider that the Cu–OOH species can directly attack the substrates in a concerted manner^{13,31} prior to the O–O bond scission as the previously proposed mechanism of D β M^{6a} and PHM.⁹ Whether the O–O bond of the hydroperoxy species is cleaved prior to the substrate oxidation in the catalytic cycles of D β M and PHM is a point of current debate.

(50) Taylor, R. C.; Cross, P. C. *J. Chem. Phys.* **1956**, *24*, 41.

(51) Kitagawa, T.; Ondrias, M. R.; Rousseau, R. L.; Ikeda-Saito, M.; Yonetani, T. *Nature (London)* **1982**, *298*, 869.

Table 7. Extended Hückel Parameters for Cu, S, C, N, and H Atoms

orbital	H_{ii} (eV)	ζ_{ii}	(c1)	ζ_{i2}	(c2)
Cu 4s	-11.4	2.2			
Cu 4p	-6.06	2.2			
Cu 3d	-14.0	5.95	(0.5933)	2.30	(0.5744)
S 3d	-8.0	1.500			
S 3p	-11.0	1.827			
S 3s	-20.0	2.122			
C 2s	-21.4	1.625			
C 2p	-11.4	1.625			
N 2s	-26.0	1.950			
N 2p	-13.4	1.950			
H 1s	-13.6	1.3			

Conclusions

Complexes **1** and **2** mediated H₂O₂-dependent selective conversions of cyclohexane to cyclohexanol in a metal-based oxidation manner, while **3**/H₂O₂ oxidized the hydrocarbons in a radical manner. Furthermore, the **1**/H₂O₂ combination catalyzed the cyclohexene epoxidation, which may have relevance to the oxidation chemistry of D β M, while **2**/H₂O₂ did not catalyze it. We have spectroscopically characterized the hydroperoxy–copper species in the reaction mixture of **1** with H₂O₂, in which the O–O bonds are significantly activated compared with the previously reported Cu–OOH species. While, as demonstrated by the [Fe(TPA)(OOH)]²⁺ complex,⁴⁵ mononuclear iron enzymes can utilize the low-spin nature of the iron centers to weaken the O–O bond of the hydroperoxy species, the mononuclear center of copper-containing monooxygenases may have to employ the strong donor ligand to weaken the O–O bond for O atom transfers to substrates because a spin state alternation is not accessible by the d⁹ configuration of the Cu(II) centers. Further studies to unravel the nature of the Cu–OOH species are under way.

Acknowledgment. K.Y. and T.K. acknowledge a Grant-in-Aid for Scientific Research on the Priority Area “Molecular Biometallics” from the Ministry of Education, Science, Sports and Culture of Japan. This work was partly supported by the “Research for the Future” Program from the Japan Society for the Promotion of Science (Grant JSPS-RFTF96P00206). Thanks are due to Ms. Sachiyo Nomura and Dr. Hideki Fujiwara of the Institute for Molecular Science for their kind help in measurements of FAB and ESI mass spectra. We are grateful to Mr. Shiro Yoshioka and Professor Isao Morishima for their help in using the UV–vis spectrometer. T.O. is grateful to the JSPS for a graduate fellowship.

Appendix

Structural parameters used for **4**, **5a**, and **5b** are listed in Table 6, and extended Hückel parameters used for copper, sulfur, nitrogen, carbon, and hydrogen atoms appear in Table 7.

Supporting Information Available: X-ray crystallographic files, in CIF format, for complexes **1** and **2**. This material is available free of charge via the Internet at <http://pubs.acs.org>.

IC000018A